Available online at www.sciencedirect.com
SCIENCE DIRECT®
Annals of Physics 315 (2005) 52–79
ANNALS of PHYSICS
www.elsevier.com/locate/aop

The cold atom Hubbard toolbox

D. Jaksch[a,b,*], P. Zoller[b]

[a] Clarendon Laboratory, University of Oxford, Parks Road, Oxford OX1 3PU, UK
[b] Institute for Theoretical Physics, University of Innsbruck, and Institute for Quantum Optics and Quantum Information of the Austrian Academy of Sciences, 6020 Innsbruck, Austria

Received 31 August 2004; accepted 28 September 2004
Available online 19 December 2004

Abstract

We review recent theoretical advances in cold atom physics concentrating on strongly correlated cold atoms in optical lattices. We discuss recently developed quantum optical tools for manipulating atoms and show how they can be used to realize a wide range of many body Hamiltonians. Then, we describe connections and differences to condensed matter physics and present applications in the fields of quantum computing and quantum simulations. Finally, we explain how defects and atomic quantum dots can be introduced in a controlled way in optical lattice systems.

PACS: 03.75.−b; 32.80.Pj; 32.80.Qk; 03.67.Lx
Keywords: Cold atom; Optical lattice; Hubbard model; Quantum computing; Atomic quantum dot

1. Introduction

Atomic physics experiments with quantum degenerate Bose and Fermi gases are characterized by the distinguishing features that we have: (i) a detailed microscopic understanding of the Hamiltonian of the systems realized in the laboratory, and (ii) complete control of the system parameters via external fields. In particular, atoms can be trapped and their motion controlled in magnetic and optical traps, allowing,

* Corresponding author. Fax: +44 1865 272375.
E-mail address: Dieter.Jaksch@physics.ox.ac.uk (D. Jaksch).

0003-4916/$ - see front matter © 2004 Elsevier Inc. All rights reserved.
doi:10.1016/j.aop.2004.09.010

for example, the realization of quantum gases with different dimensionality at effectively zero temperature. In addition, atoms have many internal states which can be manipulated using laser light and can be employed as a probe of the gas properties, and their collisional properties can be tuned with magnetic and optical Feshbach resonances.

In the early days of atomic BEC experiments [1–5], the main focus was to investigate condensate properties of matter waves like coherence, as described theoretically by the Hartree–Fock–Bogoliubov mean field theory for weakly interacting quantum gases. More recently, emphasis has shifted to strongly interacting systems, which are much more in line with present interests in theoretical condensed matter physics. In particular, as first pointed out in [6], strongly interacting systems can be realized with cold atomic gases in optical lattices, i.e., periodic arrays of microtraps generated by standing wave laser light fields. This leads to Hubbard type lattice models, where atomic physics provides a whole toolbox to engineer various types of Hamiltonians for 1D, 2D, and 3D Bose and Fermi systems which can be controlled by varying external field parameters in a time dependent way. In addition, atomic physics provides systematic ways of loading these lattices with atoms. A prominent example is the Mott insulator-superfluid quantum phase transition with cold bosonic atoms, as first observed in the seminal experiment by Bloch and collaborators [7]. More generally, we expect that cold atoms in optical lattices will be developed in the coming years as a general quantum simulator of lattice models, allowing experimental insight into phase diagrams for certain classes of (toy) models (such as high-T_c superconductivity) and for parameter regimes, where no rigorous theoretical approaches exist. In addition, new theoretical challenges appear in this context, for example, the study of time-dependent phenomena. Besides the condensed matter aspects, the engineered Hubbard models have direct application in quantum computing, where the controlled interactions can be used to create entanglement with high fidelity.

In the present article, we discuss the atomic physics point of developing a Hubbard toolbox by controlling laser and collisional interactions [8]. The basic physical mechanisms for creating periodic optical trapping potentials are introduced in Section 2. In Section 3, we discuss some of the various Hubbard models that can be engineered in optical lattices and also give a microscopic explanation of the terms appearing in the Hamiltonians. Then, we point out the similarities and in particular the novel aspects in comparison to condensed matter systems in Section 4, and proceed by describing possible applications in quantum computing and quantum simulations in Section 5. Finally, some prospects for introducing imperfections and quantum dots into optical lattices are discussed in Section 6 and we conclude in Section 7.

2. Optical lattices

Lasers are a very versatile tool for manipulating atoms. Atoms may be cooled or can even be trapped by laser light [9]. For trapping the purely conservative dipole force exerted by a laser with an inhomogeneous intensity profile is used [10]. In this section, we present several examples of different laser–atom configurations which

allow the realization of a variety of trapping potential, in particular periodic optical lattices with different geometries, and even trapping potentials whose shape depends on the internal (hyperfine) state of the atom. In our derivations, we will neglect spontaneous emission and later establish the consistency of this approximation by giving an estimate for the rate at which photons are spontaneously emitted in a typical optical lattice setup.

2.1. Optical potentials

The Hamiltonian of an atom of mass m is given by $H_A = \mathbf{p}^2/2m + \sum_j \omega_j |e_j\rangle\langle e_j|$. Here, $\mathbf{p}$ is the center of mass momentum operator and $|e_j\rangle$ denote the internal atomic states with energies ω_j (setting $\hbar \equiv 1$). We assume the atom to initially occupy a metastable internal state $|e_0\rangle \equiv |a\rangle$ which defines the point of zero energy. The atom is subject to a classical laser field with electric field $\mathbf{E}(\mathbf{x},t) = E(\mathbf{x},t)\epsilon \exp(-\mathrm{i}\omega t)$, where ω is the frequency and ϵ the polarization vector of the laser. The amplitude of the electric field $E(\mathbf{x},t)$ is varying slowly in time t compared to $1/\omega$ and slowly in space $\mathbf{x}$ compared to the size of the atom. In this situation the interaction between atom and laser is adequately described in dipole approximation by the Hamiltonian $H_{\mathrm{dip}} = -\mu\mathbf{E}(\mathbf{x},t) + \mathrm{h.c.}$, where μ is the dipole operator of the atom. We assume the laser to be far detuned from any optical transition so that no significant population is transferred from $|a\rangle$ to any of the other internal atomic states via H_{dip}. We can thus treat the additional atomic levels in perturbation theory and eliminate them from the dynamics. In doing so we find the AC-Stark shift of the internal state $|a\rangle$ in the form of a conservative potential $V(\mathbf{x})$ whose strength is determined by the atomic dipole operator and the properties of the laser light at the center of mass position $\mathbf{x}$ of the atom. In particular $V(\mathbf{x})$ is proportional to the laser intensity $|E(\mathbf{x},t)|^2$. Under these conditions the motion of the atom is governed by the Hamiltonian $H = \mathbf{p}^2/2m + V(\mathbf{x})$.

Let us now specialize the situation to the case where the dominant contribution to the optical potential arises from one excited atomic level $|e\rangle$ only. In a frame rotating with the laser frequency the Hamiltonian of the atom is approximately given by $H_{\mathrm{A}} = \mathbf{p}^2/2m + \delta|e\rangle\langle e|$, where $\delta = \omega_e - \omega$ is the detuning of the laser from the atomic transition $|e\rangle \leftrightarrow |a\rangle$. The dominant contribution to the atom–laser interaction neglecting all quickly oscillating terms (i.e., in the rotating wave approximation) is given by $H_{\mathrm{dip}} = \Omega(\mathbf{x})|e\rangle\langle a|/2 + \mathrm{h.c.}$ Here $\Omega = -2\ E(\mathbf{x},t)\langle e|\mu\epsilon|a\rangle$ is the so-called Rabi frequency driving the transitions between the two atomic levels. For large detuning $\delta \gg \Omega$ adiabatically eliminating the level $|e\rangle$ yields the explicit expression $V(\mathbf{x}) = |\Omega(\mathbf{x})|^2/4\delta$ for the optical potential. The population transferred to the excited level $|e\rangle$ by the laser is given by $|\Omega(\mathbf{x})|^2/4\delta^2$ and this is the reason why we require $\Omega(\mathbf{x}) \ll \delta$ for our adiabatic elimination to be valid.

2.2. Periodic lattices

For creating an optical lattice potential we start by superimposing two counter propagating running wave laser beams with $E_{\pm}(\mathbf{x},t) = E_0 \exp(\pm\,\mathrm{i}kx)$ propagating in x-direction with amplitude E_0, wave number k and wave length $\lambda = 2\pi/k$. They

create an optical potential $V(\mathbf{x}) \propto \cos^2(kx)$ in one dimension with periodicity $a = \lambda/2$. Using two further pairs of laser beams propagating in y and z direction, respectively, a full three-dimensional periodic trapping potential of the form

$$V(\mathbf{x}) = V_{0x}\cos^2(kx) + V_{0y}\cos^2(ky) + V_{0z}\cos^2(kz) \tag{1}$$

is realized. The depth of this lattice in each direction is determined by the intensity of the corresponding pair of laser beams which is easily controlled in an experiment.

2.2.1. Bloch bands and Wannier functions

For simplicity we only consider one spatial dimension in Eq. (1) and write down the Bloch functions $\phi_q^{(n)}(x)$ with q the quasi momentum and n the band index. The corresponding eigenenergies $E_q^{(n)}$ for different depths of the lattice V_0/E_R in units of the recoil energy $E_R = k^2/2m$ are shown in Fig. 1. Already for a moderate lattice depth of a few recoil the separation between the lowest lying bands is much larger than their extend. In this case a good approximation for the gap between these bands is given by the oscillation frequency ω_T of a particle trapped close to one of the minima x_j (≡ lattice site) of the optical potential. Approximating the lattice around a minimum by a harmonic oscillator we find $\omega_T = \sqrt{4V_0E_R}$ [6].

The dynamics of particles moving in the lowest lying well separated bands will be described using Wannier functions. These are complete sets of orthogonal normalized real mode functions for each band n. For properly chosen phases of the $\phi_q^{(n)}(x)$ the Wannier functions optimally localized at lattice site x_j are defined by Kohn [11]

$$w_n(x - x_j) = \Theta^{-1/2} \sum_q \mathrm{e}^{-\mathrm{i}qx_j} \phi_q^{(n)}(x), \tag{2}$$

where Θ is a normalization constant. Note that for $V_0 \to \infty$ and fixed k the Wannier function $w_n(x)$ tends towards the wave function of the nth excited state of a harmonic oscillator with ground state size $a_0 = \sqrt{1/m\omega_T}$. We will use the Wannier functions to describe particles trapped in the lattice since they allow: (i) to attribute a

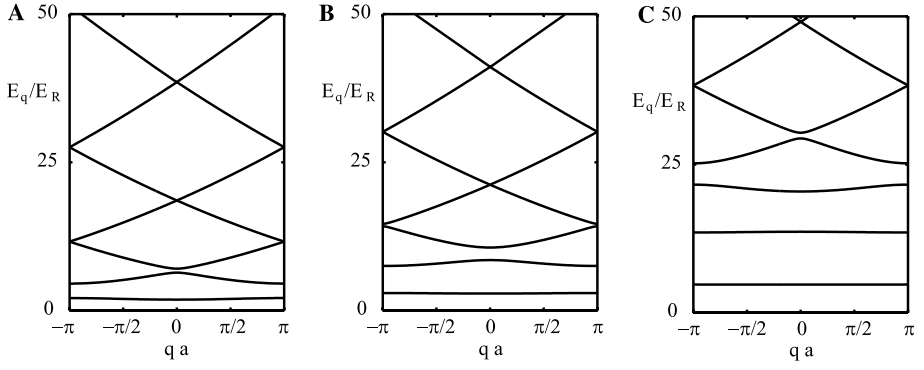

Fig. 1. Band structure of an optical lattice of the form $V_0(x) = V_0\cos^2(kx)$ for different depths of the potential: (A) $V_0 = 5E_R$, (B) $V_0 = 10E_R$, and (C) $V_0 = 25E_R$.

mean position x_j to the particles in a given mode and (ii) to easily account for local interactions between particles since the dominant contribution to the interaction energy arises from particles occupying the same lattice site x_j.

2.2.2. Lattice geometry

The lattice site positions $\mathbf{x}_j$ determine the lattice geometry. For instance the above arrangement of three pairs of orthogonal laser beams leads to a simple cubic lattice (shown in Fig. 2A). Since the laser setup is very versatile different lattice geometries can be achieved easily. As one example consider three laser beams propagating at angles $2\pi/3$ with respect to each other in the xy-plane and all of them being polarized in z direction. The resulting lattice potential is given by $V(\mathbf{x}) \propto 3 + 4\cos(3kx/2)\cos(\sqrt{3}ky/2) + 2\cos(\sqrt{3}ky)$ which is a triangular lattice in two dimensions. An additional pair of lasers in z direction can be used to create localized lattice sites (cf. Fig. 2B). Furthermore, as will be discussed later in Section 3, the motion of the atoms can be restricted to two or even one spatial dimension by large laser intensities. As will be shown it is thus possible to create truly one- and two-dimensional lattice models as indicated in Figs. 2B and C.

2.2.3. Pseudo random site offset

This can be achieved by additional superlattice potentials. Two additional laser beams propagating at small angles α and at $\pi-\alpha$ with respect to the x-axis of the lattice, respectively, superimpose a slowly varying potential with spatial period $l = \sin(\alpha)/2\bar{k}$ where $\bar{k}$ is the wave number of the additional lasers. If $l \gg a$ the main effect of the superlattice is an energy offset $\epsilon_i \propto \cos(x_i/l)$ for lattice site $\mathbf{x}_i$. If the periodicity l is incommensurate with a and several additional lasers with different periodicity l_n are superimposed to the original lattice the site offsets ϵ_i can be made quasi random over the size of the actual optical lattice.

2.2.4. State dependent lattices

As already mentioned above the strength of the optical potential crucially depends on the atomic dipole moment between the internal states involved. Thus we can exploit selection rules for optical transitions to create differing traps for different

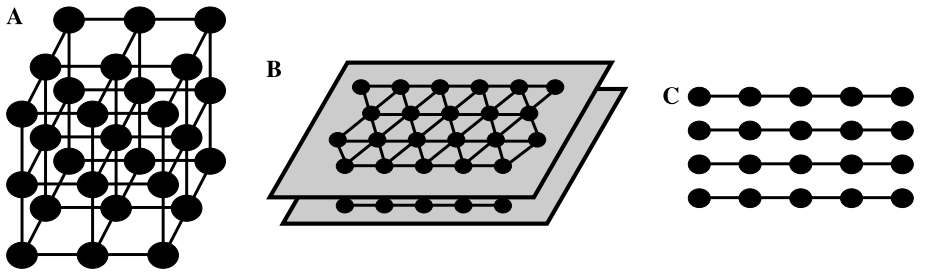

Fig. 2. (A) Simple three-dimensional cubic lattice. (B) Sheets of a two-dimensional triangular lattice. (C) Set of one-dimensional lattice tubes. In (A)–(C) tunnelling of atoms through the optical potential barriers is only possible between sites which are connected by lines.

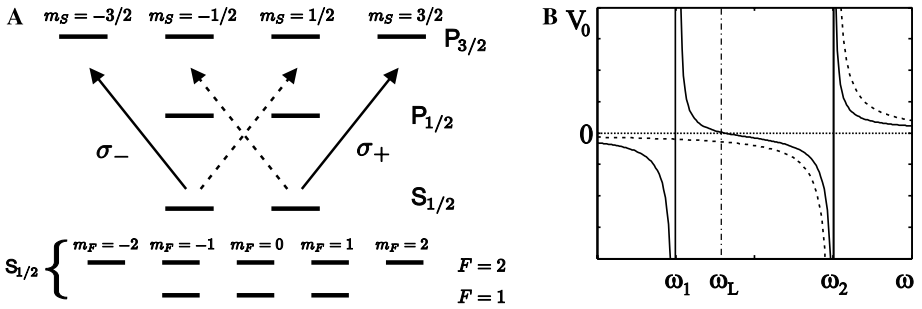

Fig. 3. (A) Atomic fine and hyperfine structure of the most commonly used alkali atoms ^{23}Na and ^{87}Rb. (B) Schematic AC-Stark shift of the atomic level $S_{1/2}$ with $m_s = 1/2$ (dashed curve) and with $m_s = -1/2$ (solid curve) due to the laser beam σ_+ as a function of the laser frequency ω. The AC-Stark shift of the level $S_{1/2}$ with $m_s = -1/2$ can be made 0 by choosing the laser frequency $\omega = \omega_L$.

internal states of the atom [12–14]. We will illustrate this by an example that is particularly relevant in what follows. We consider an atom with the fine structure shown in Fig. 3A, like, e.g., ^{23}Na or ^{87}Rb, interacting with two circularly polarized laser beams. The right circularly polarized laser σ^+ couples the level $S_{1/2}$ with $m_s = -1/2$ to two excited levels $P_{1/2}$ and $P_{3/2}$ with $m_s = 1/2$ and detunings of opposite sign. The respective optical potentials add up. The strength of the resulting AC-Stark shift is shown in Fig. 3B as a function of the laser frequency ω. For $\omega = \omega_L$ the two contribution cancel. The same can be achieved for the σ^- laser acting on the $S_{1/2}$ level with $m_s = 1/2$. Therefore at $\omega = \omega_L$ the AC-Stark shifts of the levels $S_{1/2}$ with $m_s = \pm 1/2$ are purely due to $\sigma_\pm$ polarized light which we denote by $V_\pm(x)$. The corresponding level shifts of the hyperfine states in the $S_{1/2}$ manifold (shown in Fig. 3A) are related to $V_\pm(x)$ by the Clebsch–Gordan coefficients, e.g., $V_{|F=2,m_F=2\rangle}(x) = V_+(x)$, $V_{|F=1,m_F=1\rangle}(x) = 3V_+(x)/4 + V_-(x)/4$, and $V_{|F=1,m_F=-1\rangle}-(x) = V_+(x)/4 + 3V_-(x)/4$.

2.2.5. State selectively moving the lattice

The two standing waves $\sigma_\pm$ can be produced out of two running counter-propagating waves with the same intensity as shown in Fig. 4. Moreover it is possible to move nodes of the resulting standing waves by changing the angle of the polarization between the two running waves [12]. Let $\{e_1, e_2, e_3\}$ be three unit vectors in space pointing along the $\{x, y, z\}$ direction, respectively. The position dependent part of the electric field of the two running waves $\mathbf{E}_{1,2}$ is given by $\mathbf{E}_1 \propto e^{ikx}(\cos(\varphi)e_3 + \sin(\varphi)e_2)$, $\mathbf{E}_2 \propto e^{-ikx}(\cos(\varphi)e_3 - \sin(\varphi)e_2)$. The sum of the two electric fields is thus $\mathbf{E}_1 + \mathbf{E}_2 \propto \cos(kx-\varphi)\sigma_- - \cos(kx+\varphi)\sigma_+$, where $\sigma_\pm = e_2 \pm ie_3$ and the resulting optical potentials are given by

$$V_\pm(x) \propto \cos^2(kx \pm \varphi). \tag{3}$$

By changing the angle φ it is therefore possible to move the nodes of the two standing waves in opposite directions. Since these two standing waves act as internal state

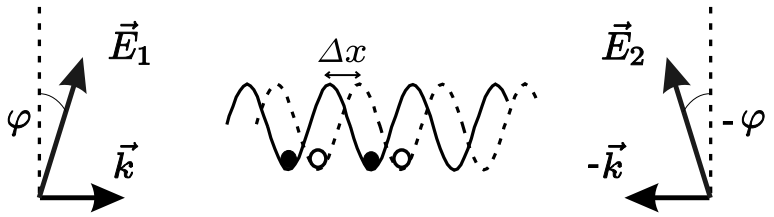

Fig. 4. Laser configuration for a state selective optical potential. Two standing circular polarized standing waves are produced out of two counter-propagating running waves with an angle 2φ between their polarization axes. The lattice sites for different internal states (indicated by closed and open circles) are shifted by $\Delta x = 2\varphi/k$.

dependent potentials for the hyperfine states the optical lattice can be moved in opposite directions for different internal hyperfine states.

2.2.6. Population transfer between hyperfine states

Two atomic hyperfine levels can be coupled coherently via magnetic dipole moment matrix elements by an additional oscillating microwave field. Alternatively transitions can also be driven by a Raman laser setup which consists of two laser beams and couples two hyperfine levels via a far detuned excited state. In both cases the dynamics is described by a Hamiltonian of the form $H_{\mathrm{R}} = (\Omega_{\mathrm{R}}|a\rangle\langle b| + \mathrm{h.c.})/2 + \delta_{\mathrm{R}}|b\rangle\langle b|$ with Ω_{R} the Rabi frequency, δ_{R} the detuning and $|a\rangle$, $|b\rangle$ the two coupled atomic states.

2.3. Validity

In all of the above calculations we have only considered the coherent interactions of an atom with laser light. Any incoherent scattering processes which lead to spontaneous emission were neglected. We will now establish the validity of this approximation by estimating the mean rate Γ_{eff} of spontaneous photon emission from an atom trapped in the lowest vibrational state of the optical lattice. This rate of spontaneous emission is given by the product of the life time Γ of the excited state and the probability of the atom occupying this state. In the case of a blue detuned optical lattice (dark optical lattice) $\delta < 0$ the potential minima coincide with the points of no light intensity and we find the effective spontaneous emission rate $\Gamma_{\mathrm{eff}} \approx -\Gamma\omega_T/4\delta$. If the lattice is red detuned (bright optical lattice) $\delta > 0$ the potential minima match the points of maximum light intensity and we find $\Gamma_{\mathrm{eff}} \approx \Gamma V_0/\delta$. Since $V_0 > \omega_T$ the spontaneous emission in a red detuned optical lattice will always be more significant than in a blue lattice, however, as long as $V_0 \ll \delta$ spontaneous emission does not play a significant role.

2.3.1. Typical numerical values

In a typical blue detuned optical lattice with $\lambda = 514$ nm for ^{23}Na atoms ($S_{1/2}$–$P_{3/2}$ transition at $\lambda_2 = 589$ nm and $\Gamma = 2\pi \times 10$ MHz) the recoil energy is $E_{\mathrm{R}} \approx$

$2\pi \times 33$ kHz and the detuning from the atomic resonance is $\delta \approx -2.3 \times 10^9 E_R$. A lattice with depth $V_0 = 25E_R$ leads to a trapping frequency of $\omega_T = 10E_R$ yielding a spontaneous emission rate of $\Gamma_{\text{eff}} \approx 10^{-2}/s$ while experiments are typically carried out in times shorter than 1 s. Therefore spontaneous emission does not play a significant role in such experiments.

3. The (Bose) Hubbard model

We consider a gas of interacting particles moving in an optical lattice. Starting from the full many body Hamiltonian including local two particle interactions we first give a naive derivation of the Bose-Hubbard model (BHM) [15,6] and present related models which can be realized in an optical lattice. Then we proceed by discussing adiabatic and irreversible schemes for loading the lattice with ultracold atoms. Finally, we examine the microscopic origin of the interaction terms appearing in the BHM. Throughout, we will mostly concentrate on bosonic atoms, however, similar derivations can also be performed for fermions [14,16] and we will also give one example of such a fermionic model.

3.1. Naive derivation of the BHM

The Hamiltonian of a weakly interacting gas in an optical lattice is

$$H_{\text{full}} = \int \mathrm{d}^3 x \hat{\Psi}^\dagger(\mathbf{x}) \left(\frac{\mathbf{p}^2}{2m} + V_0(\mathbf{x}) + V_T(\mathbf{x}) \right) \hat{\Psi}(\mathbf{x}) + \frac{g}{2} \int \mathrm{d}x \hat{\Psi}^\dagger(\mathbf{x}) \hat{\Psi}^\dagger(\mathbf{x}) \hat{\Psi}(\mathbf{x}) \hat{\Psi}(\mathbf{x}) \tag{4}$$

with $\hat{\Psi}(\mathbf{x})$ the bosonic field operator for atoms in a given internal atomic state $|b\rangle$ and $V_T(\mathbf{x})$ a (slowly varying compared to the optical lattice $V_0(\mathbf{x})$) external trapping potential, e.g., a magnetic trap or a superlattice potential. The parameter g is the interaction strength between two atomic particles. If the atoms interact via s-wave scattering only it is given by $g = 4\pi a_s/m$ with a_s the s-wave scattering length. We assume all particles to be in the lowest band of the optical lattice and expand the field operator in terms of the Wannier functions $\hat{\Psi}(\mathbf{x}) = \sum_i \hat{b}_i w^{(0)}(\mathbf{x} - \mathbf{x}_i)$, where $\hat{b}_i$ is the destruction operator for a particle in site $\mathbf{x}_i$. We find $H_{\text{full}} = -\sum_{i,j} J_{ij} \hat{b}_i^\dagger \hat{b}_j + \frac{1}{2} \sum_{i,j,k,l} U_{ijkl} \hat{b}_i^\dagger \hat{b}_j^\dagger \hat{b}_k \hat{b}_l$, where

$$J_{ij} = -\int \mathrm{d}x w_0(\mathbf{x} - \mathbf{x}_i) \left(\frac{p^2}{2m} + V_0(\mathbf{x}) + V_T(\mathbf{x}) \right) w_0(\mathbf{x} - \mathbf{x}_j),$$

and

$$U_{ijkl} = g \int \mathrm{d}x w_0(\mathbf{x} - \mathbf{x}_i) w_0(\mathbf{x} - \mathbf{x}_j) w_0(\mathbf{x} - \mathbf{x}_k) w_0(\mathbf{x} - \mathbf{x}_l).$$

The numerical values for the offsite interaction matrix elements U_{ijkl} involving Wannier functions centered at different lattice sites as well as tunnelling matrix elements J_{ij} to sites other than nearest neighbors (note that diagonal tunneling is not allowed

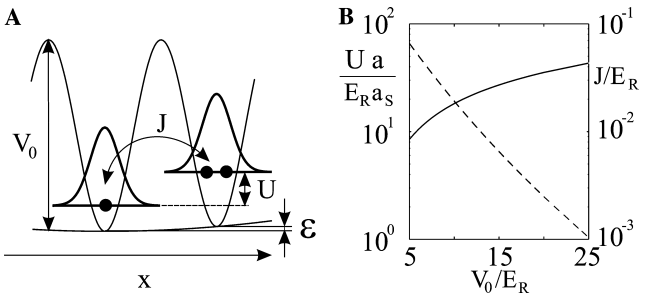

Fig. 5. (A) Interpretation of the BHM in an optical lattice as discussed in the text. (B) Plot of scaled onsite interaction U/E_R multiplied by a/a_s ($\gg 1$) (solid line with axis on left-hand side of graph) and J/E_R (dashed line, with axis on right-hand side of graph) as a function of $V_0/E_R \equiv V_{x,y,z_0}/E_R$ (for a cubic 3D lattice).

in a cubic lattice since the Wannier functions are orthogonal) are small compared to onsite interactions $U_{0000} \equiv U$ and nearest neighbor tunneling $J_{01} \equiv J$ for reasonably deep lattices $V_0 \gtrsim 5E_R$. We can therefore neglect them and for an isotropic cubic optical lattice arrive at the standard Bose–Hubbard Hamiltonian

$$H_{BH} = -J \sum_{\langle i,j \rangle} \hat{b}_i^\dagger \hat{b}_j + \frac{U}{2} \sum_j \hat{b}_j^\dagger \hat{b}_j^\dagger \hat{b}_j \hat{b}_j + \sum_j \epsilon_j \hat{b}_j^\dagger \hat{b}_j. \tag{5}$$

Here $\langle i,j \rangle$ denotes the sum over nearest neighbors and the terms $\epsilon_j = V_T(\mathbf{x}_j)$ arise from the additional trapping potential. The physics described by H_{BH} is schematically shown in Fig. 5A. Particles gain an energy of J by hopping from one site to the next while two particles occupying the same lattice site provide an interaction energy U. An increase in the lattice depth V_0 leads to higher barriers between the lattice sites decreasing the hopping energy J as shown in Fig. 5B. At the same time two particles occupying the same lattice site become more compressed which increases their repulsive energy U (cf. Fig. 5B).

3.1.1. Tunneling term J

In the case of an ideal gas where $U = 0$ the eigenstates of H_{BH} are easily found for $\epsilon_i = 0$ and periodic boundary conditions. From the eigenvalue equation $E_q^{(0)} = -2J\cos(qa)$ we find that $4J$ is the height of the lowest Bloch band. Furthermore we see that the energy is minimized for $q = 0$ and therefore particles in the ground state are delocalized over the whole lattice, i.e., the ground state of N particles in the lattice is $|\Psi_{SF}\rangle \propto (\sum_i \hat{b}_i^\dagger)^N |\text{vac}\rangle$ with $|\text{vac}\rangle$ the vacuum state. In this limit the system is superfluid (SF) and possesses first order long range off diagonal correlations [15,6].

3.1.2. Onsite interaction U

In the opposite limit where the interaction U dominates the hopping term J the situation changes completely. As discussed in detail in [15,6] a quantum phase transition takes place at about $U \approx 5.8zJ$ where z is the number of nearest neighbors of each lattice site. The long range correlations cease to exist in the ground state and

instead the system becomes Mott insulating (MI). For commensurate filling of one particle per lattice site this MI state can be written as $|\Psi_{\mathrm{MI}}\rangle \propto \prod_j \hat{b}_j^\dagger |\mathrm{vac}\rangle$.

3.2. Lattice geometry and spin models

The lattice geometry and dimensionality are reflected in the sum over the nearest neighbors $\langle i,j\rangle$. Exotic geometries like, e.g., a Kagome lattice can be realized [17] and disordered systems may be studied by superimposing a pseudorandom potential [18]. If for the simple cubic lattice the laser intensities in z and y direction are made very large compared to the intensity in x tunnelling predominantly happens along the x direction (cf. Fig. 5) and the system is effectively reduced to a set of one dimensional lattices. In addition, when the laser intensities are turned on sufficiently slowly (adiabatically), the correlations between atoms in different optical lattice tubes cease via the SF to MI transition and the experimental setup becomes an ensemble of independent one dimensional systems. These can be used to study properties of strongly correlated gases like, e.g., a Tonks-Girardeau gas recently experimentally achieved in [19], or the excitation spectrum of one dimensional ultracold gases [20].

3.2.1. Spin models

If several species of atoms, e.g., different hyperfine states, are trapped in the lattice one often identifies them with spin degrees of freedom. The most common example is a spin 1/2 system created from two states $|\downarrow\rangle \equiv |a\rangle$ and $|\uparrow\rangle \equiv |b\rangle$. Such systems possess rich phase diagrams [21] and as shown in [22–24] one can engineer spin exchange interactions and design their properties like anisotropy and sign by proper choices of optical potentials. It is even possible to create Cooper pairs of bosonic atoms and realize the regime of a Luttinger liquid [25].

For a lattice of fermionic atoms, using similar setups as discussed above and an additional Raman laser Ω_{R}, one can realize spin dependent Fermi Hubbard models [16,14] with, e.g., a Hamiltonian

$$H = -\sum_{\sigma\langle i,j\rangle} J_\sigma \left(\hat{c}_{\sigma i}^\dagger \hat{c}_{\sigma j} + \mathrm{h.c.}\right) - \frac{\delta_{\mathrm{R}}}{2}\sum_i \left(\hat{c}_{\uparrow i}^\dagger \hat{c}_{\uparrow i} - \hat{c}_{\downarrow i}^\dagger \hat{c}_{\downarrow i}\right) + \frac{\Omega_{\mathrm{R}}}{2}\sum_i \left(\hat{c}_{\uparrow i}^\dagger \hat{c}_{\downarrow i} + \mathrm{h.c.}\right) - U\sum_i \hat{c}_{\uparrow i}^\dagger \hat{c}_{\downarrow i}^\dagger \hat{c}_{\downarrow i}\hat{c}_{\uparrow i}, \tag{6}$$

where $\hat{c}_{\sigma j}(\hat{c}_{\sigma j}^\dagger)$ destroys (creates) a fermion in lattice site j and internal state $\sigma \in \{\uparrow,\downarrow\}$ and the hopping matrix element J_σ can be made spin dependent by state selective optical potentials. Also loading of mixtures of bosonic and fermionic atoms into an optical lattice was proposed, the phase diagram was worked out [26] and effects like pairing of fermions with bosons [27] or the phase separation of the two species [28] were studied.

3.2.2. The Hofstaedter butterfly

A slightly more involved laser setup even allows for the realization of effective magnetic fields in two-dimensional optical lattices [29]. This requires time reversal

symmetry to be broken which can, e.g., be achieved by a combination of accelerating a state dependent lattice and using Raman lasers to induce the hopping between sites as schematically shown in Fig. 6. A particle moving around one plaquette of the lattice acquires a phase shift that is purely determined by the laser phases and thus can be chosen freely between $2\pi\alpha \in [0, 2\pi]$ [29]. It corresponds to a magnetic flux of $\Phi = 2\pi\alpha/e$ (with e the electron charge) and the dynamics is therefore identical to an electron moving in a lattice subject to an external magnetic field. Any strength of the magnetic field—an in particular also very large field strengths—can be achieved in the optical lattice setup and thus it should be possible to obtain the fractal energy band structure (the Hofstaedter butterfly) predicted by Hofstaedter for lattice electrons moving in huge magnetic fields [30]. Such optical lattice setups also allow for investigations of fractional quantum Hall states [31].

In this article, we exclusively discuss the case of tight optical confinement in all three dimensions with few particles per lattice site and the resulting Hubbard models. The situation where only one or two pairs of laser beams are used to create arrays of coupled BECs is instead similar to arrays of Josephson junctions. Such setups have been investigated intensively both theoretically [32–34,4] as well as experimentally [35,36]. Also early experiments which used purely optical cooling and loading methods to prepare atoms in the lowest Bloch band of the lattice and hence achieved small filling factors of approximately 10% are not considered here. For such fillings interaction effects are not important and one particle effects like Bloch oscillations, quantum chaos, and laser cooling (see, e.g. [37,38]) were of main interest in these experiments.

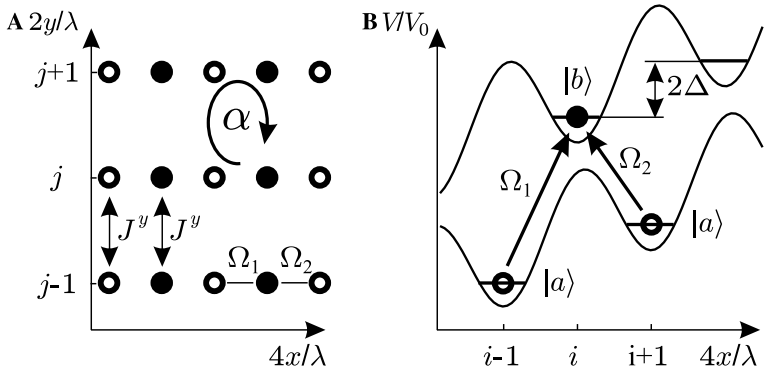

Fig. 6. Optical lattice setup: Open (closed) circles denote atoms in state $|a\rangle$ ($|b\rangle$). (A) Hopping in the y-direction is due to kinetic energy and described by the hopping matrix element J^y being the same for particles in states $|a\rangle$ and $|b\rangle$. Along the x-direction hopping amplitudes are due to the additional lasers Ω_1 and Ω_2. (B) Trapping potential in x-direction. Adjacent sites are set off by an energy Δ because of the acceleration or a static inhomogeneous electric field. The laser Ω_1 is resonant for transitions $|a\rangle \leftrightarrow |b\rangle$ while Ω_2 is resonant for transitions between $|b\rangle \leftrightarrow |a\rangle$ due to the offset of the lattice sites. Because of a spatial dependence of $\Omega_{1,2}$ in y-direction atoms hopping around one plaquette get phase shifts of $2\pi\alpha$.

3.3. Loading schemes

Only by using atomic Bose-Einstein condensates (BEC) has it become possible to achieve large densities corresponding to a few particles per lattice site. A BEC can be loaded from a magnetic trap into a lattice by slowly turning on the lasers and superimposing the lattice potential over the trap. The system adiabatically undergoes the transition from the SF ground state of the BEC to the MI state for a deep optical lattice [6]. Note that the adiabaticity condition can easily be fulfilled in this scenario since the changing optical lattice potential does not induce significant quasi-momenta and therefore the relevant energy is the distance to the excited band. Experimentally this loading scheme and the SF to MI transition was realized in several experiments [7,20,39] and led to a MI with up to two particles per lattice site. The number of defects in the created 'optical crystals' were limited to approximately 10% of the sites.

3.3.1. Defect suppressed optical lattices

One method to further decrease the number of defects in the lattice was recently described in [40]. The proposed setup utilizes two optical lattices for internal states $|a\rangle$ and $|b\rangle$ with substantially different interaction strengths $U_b \neq U_a$ and identical lattice site positions $\mathbf{x}_i$. Initially atoms in $|a\rangle$ are adiabatically loaded into the lattice and brought into a MI state where the number of particles per site may vary between $n = 1, \ldots, n_{\max}$ because of defects. Then a Raman laser with a detuning varying slowly in time between δ_i and δ_f is used to adiabatically transfer exactly one particle from $|a\rangle$ to $|b\rangle$ as shown in Figs. 7A and B. This is done by going through exactly one

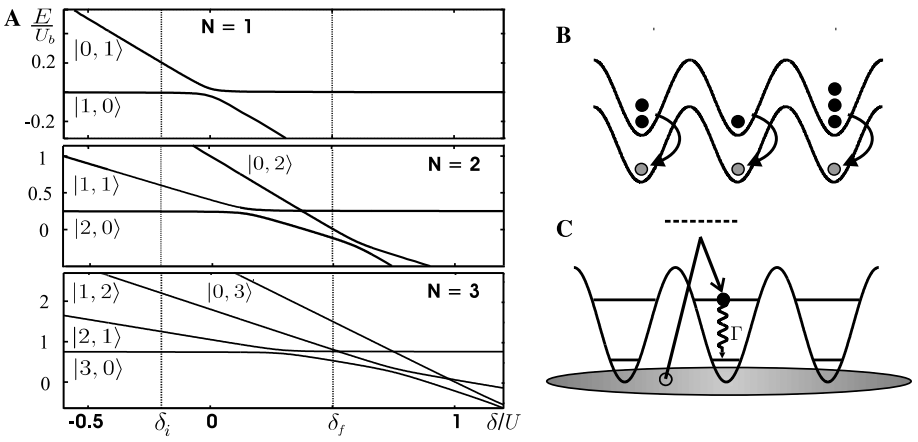

Fig. 7. (A) Avoided crossings in the energy eigenvalues E for $n = 1, 2, 3$. (Note the variation in the vertical scale.) For the chosen values of δ_i and δ_f (dotted vertical lines) only one avoided crossing is traversed transferring exactly one atom from $|a\rangle$ to $|b\rangle$ as schematically shown in B). (C) Loading of an atom into the first Bloch band from a degenerate gas and spontaneous decay to the lowest band via emitting a phonon into the surrounding degenerate gas.

avoided crossing. During the whole of this process transfer of further atoms is blocked by interactions. This scheme allows a significant suppression of defects and—with additional site offsets ϵ_i—can also be used for patterned loading [39] of the $|b\rangle$ lattice.

3.3.2. Irreversible loading schemes

Further improvement could be achieved via irreversible loading schemes. An optical lattice is immersed in an ultracold degenerate gas from which atoms are transferred into the first Bloch band of the lattice. By spontaneous emission of a phonon [41] the atom then decays into the lowest Bloch band as schematically shown in Fig. 7C. By atom–atom repulsion further atoms are blocked from being loaded into the lattice. This scheme can also be extended to cool atomic patterns in a lattice. In contrast to adiabatic loading schemes it has the advantage of being repeatable without removing atoms already stored in the lattice.

3.4. Microscopic picture

To obtain a better understanding of the interaction term U we consider two atoms trapped in one lattice site neglecting the tunnelling term J. We approximate the lattice potential by a harmonic oscillator which decouples the center of mass motion from the relative motion. While the center of mass coordinate moves in a harmonic potential of frequency ω_T the potential of the relative coordinate $\mathbf{r}$ is the sum of a harmonic trap with frequency ω_T and the interatomic interaction potential $V_{\text{int}}(\mathbf{r})$ as schematically shown in Fig. 8. The potentials $V_{\text{int}}(\mathbf{r})$ are well known and one can calculate the energy levels ε_l with good precision [42–44]. The interaction matrix element U can then be identified with the difference in energy $U = \varepsilon_l - 3\omega_T/2$ of the level l which is closest to the ground state of the bare harmonic oscillator level. The states in the Bose-Hubbard picture are thus related to the microscopic picture as

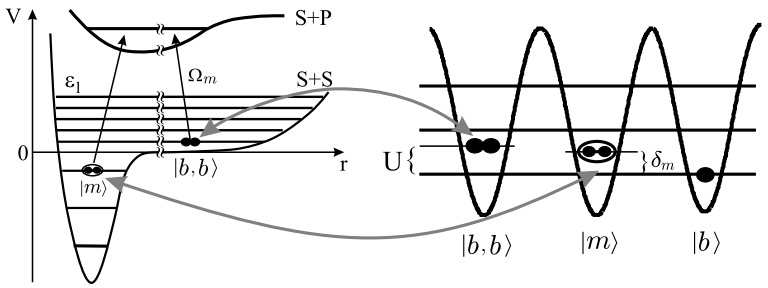

Fig. 8. Microscopic picture: the interatomic interaction plus optical potential V (not to scale) for the relative motion of two atoms. Levels above $V = 0$ are identified with two atoms in the lattice and states below $V = 0$ as molecular states since they differ significantly in their extend. The relation between levels in the Bose-Hubbard picture and in the microscopic picture are indicated by arrows. Note that we assume the optical lattice to be identical for atoms $|a\rangle$ and the molecular state $|m\rangle$ which is only true for highly excited molecular states.

indicated in Fig. 8. Also inelastic processes leading to particle loss can be treated in detail and a microscopic understanding of the behavior of U close to magnetic and optical Feshbach resonances can also be gained from this picture [42,45,46]. Based on the detailed knowledge of the two particle levels quantum optical schemes for the photoassociation of two atoms in $|a\rangle$ to form a molecule $|m\rangle$ can be devised. For instance, as schematically shown in Fig. 8, using a set of Raman lasers for molecule creation from a two particle MI state was proposed in [47]. In comparison to customary photoassociation the motion of the atoms and the molecule are precisely controlled and the resulting dynamics is described by a Hamiltonian of the form

$$H_{\mathrm{mol}} = \left(\frac{\Omega_m}{2}\hat{b}^\dagger\hat{b}^\dagger\hat{m} + \mathrm{h.c.}\right) + \delta_m\hat{m}^\dagger\hat{m}, \tag{7}$$

with Ω_{m} the effective Rabi frequency, δ_{m} the detuning and $\hat{m}\,(\hat{m}^\dagger)$ destroying (creating) a molecule in state $|m\rangle$. As above the mode $|m\rangle$ appearing in the many particle Hamiltonian H_{mol} has a well defined microscopic origin (cf. Fig. 8). In the case of three particles occupying one lattice site analytic understanding can be obtained from Efimov states which have been used to calculate three particle loss rates and interaction properties near Feshbach resonances [48–50].

4. Condensed matter aspects

The setups discussed above realize—for the first time—strongly correlated systems of neutral atoms. They are described by Hamiltonians which have been subject to extensive investigation in condensed matter physics where numerous techniques were developed to find out about their properties. It is not the purpose of this article to review these techniques but we rather point out the most important differences between customary condensed matter systems and atoms in optical lattices.

4.1. Controllability

The theoretical models for atoms in lattices follow from a microscopic picture, the origin of every term in the Hamiltonian is well justified and can be controlled via the experimental setup. For instance, the lattice geometry and tunnelling barriers are controlled by lasers parameters and their arrangement. Additional flexibility comes from the ability to tune the interaction properties of the atoms with magnetic and optical Feshbach resonances [42,45,46]. An even larger class of condensed matter systems can be realized by exploiting the lattice as a universal quantum simulator as shown in Section 5.2.

4.2. Inhomogeneity

The size of an optical lattice is relatively small in comparison to its periodicity a with typically a few hundred lattice sites in each dimension only. Also, the lattice is

usually not enclosed in a box but it is put into a slowly varying harmonic potential which translates into a space dependent site offset (can equally well be viewed as a local chemical potential). This leads, e.g., to soft boundaries of the system (cf. Fig. 9A), or the simultaneous coexistence of spatially separated phases as shown in Fig. 9B where alternating SF and MI phases are present.

4.3. Unitary dynamics

One of the most striking differences is the excellent isolation of an optical lattice from its environment. As shown above for spontaneous emission, one of the most dominant decoherence mechanisms, the typical coherence time is on the order of seconds. The characteristic energies in the Hamiltonian lead to a unitary evolution on millisecond time scales and the external parameters like the laser intensity can be changed in even shorter times. This allows the experimental study of the unitary dynamics of strongly correlated atoms from the adiabatic to the sudden regime [7,51], a topic usually not considered in traditional condensed matter physics. To obtain a better understanding of these dynamical processes new analytical and numerical methods have to be developed. Exact numerical calculations for small systems have been performed [47,52] and also trajectory based simulation methods were developed [53,54]. By combining techniques from quantum information theory with known properties of one dimensional systems [55] it was possible to develop a numerical method, the so called time evolving block decimation algortihm (TEBD) which is related to density matrix renormalization group (DMRG) techniques [56,57], for simulating the unitary dynamics of a large class of one-dimensional lattice models. In Fig. 9C, we show results from dynamical calculations on the SF to MI transition which indicate differences from static ground state calculation in the off-diagonal elements of the one particle density matrix.

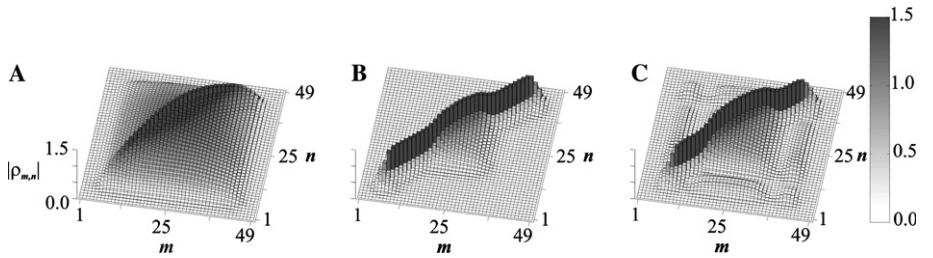

Fig. 9. Absolute values of the one particle density matrix $\rho_{m,n} = \langle \hat{b}_m^\dagger \hat{b}_n \rangle$ as a function of site indices m,n for a one-dimensional lattice superimposed by an additional slowly varying harmonic oscillator potential. All results are obtained by the TEBD [51]. (A) SF ground state for $U/2J = 2$. (B) Intermediate ground state for $U/2J = 6$. This state clearly indicates the coexistence of MI and SF states in different regions of the system. The SF region in the center of the trap is surrounded by two MI regions with one particle per lattice site followed by a small superfluid at the edges of the trap. (C) Intermediate state created from the SF by dynamically ramping up the depth of the lattice until $U/2J = 6$ [51]. Note the correlations between the two SF regions which are absent in the corresponding ground state.

4.4. Quantum state engineering

Simple condensed matter Hamiltonians like the BHM are often considered as toy models for obtaining insight into more complicated real physical systems and are thus not expected to fully describe the physics and in particular the full many body wave function. Through their exact realization with neutral cold atoms and the excellent isolation of these systems from their environment such toy models become interesting for quantum state engineering and quantum computing applications which require precise knowledge of the system wave function. Quantum optical methods provide the accurate control and manipulability and the strongly correlated nature of the system can, e.g., be exploited to initialize a quantum register [6,12], achieve increased stability [58] or even to provide the basic resource for quantum computations [59]. Some of these quantum computing implementations will be presented in Section 5.

5. Quantum computing implementations

One of the big challenges for 21st century physics is the demonstration of a quantum computer which promises a significant speed up for certain kinds of algorithms, most prominently the factorization of large numbers and searching in unsorted databases [60]. While the realization of a universal quantum computer is certainly a long-term goal, also a number of *nontrivial* applications with limited quantum computer resources exist for the nearer future in the areas of quantum communication, entanglement creation (see Section 5.1), special purpose quantum computing, or Feynman's universal quantum simulator (see Section 5.2).

The basic requirements for a physical system to be capable of quantum computing have been laid out by DiVincenzo [61]. Many of these are fulfilled for atoms in optical lattices. An optical lattice provides an intrinsically *scalable* and *well defined* set of qubits (quantum register) with *long decoherence* times. These are usually constituted by two metastable ground states of the atoms $|a\rangle$ and $|b\rangle$ trapped in the lattice. The *initialization* of the quantum register can be achieved by the loading schemes discussed above where the MI state with one particle per lattice site corresponds to the register initialized with zeros. Any quantum computation can be carried out by applying *single qubit gates* via Raman lasers, and controlled interactions between the particles to perform *two qubit gates* as described in Section 5.1 [12,13,62,63]. Also several other schemes for quantum computing in optical lattices have been proposed based on, e.g., strong dipole–dipole interactions between Rydberg atoms [64], the motional state of the atoms [65], atom tunnelling between neighboring sites [66], or measurements on highly entangled states [59]. Currently the main (technical) drawback in many of these optical lattice quantum computing schemes is the difficulty of addressing individual atoms. While a large number of quantum gate operations can already be carried out in parallel [63] it is not yet experimentally possible to perform them on selected pairs of atoms. However, proposals on utilizing marker atoms [46] or on quantum computing via global system control [67] exist and will allow to overcome this problem in the near future.

5.1. Entanglement creation via coherent ground state collisions

We exploit the two particle interaction term $g\int \mathrm{d}^3x\hat{\Psi}^\dagger(\mathbf{x})\hat{\Psi}^\dagger(\mathbf{x})\hat{\Psi}(\mathbf{x})\hat{\Psi}(\mathbf{x})/2$ from Eq. (4) whose origin lies in the atom–atom interaction potential for the controlled creation of entangled states. In optical lattices these nonlinear atom–atom interactions can be large [12], even for interactions between individual pairs of atoms. In addition, we use a state selective optical lattice potential as introduced in Section 2 to provide control over the motional states of the atoms.

Consider a situation where two atoms populating the internal states $|a\rangle$ and $|b\rangle$, respectively, are trapped in the ground states $\psi_0^{a,b}$ of two potential wells $V^{a,b}$. Initially, at time $t=-\tau$, these wells are centered at positions $\bar{x}^a$ and $\bar{x}^b$, sufficiently far apart (distance $d=\bar{x}_b-\bar{x}_a$) so that the particles do not interact (see Fig. 10A). The positions of the potentials are moved along trajectories $\bar{x}^a(t)$ and $\bar{x}^b(t)$ so that the wave packets of the atoms overlap for certain time, until finally they are restored to the initial position at $t=\tau$. This situation is described by the Hamiltonian

$$H=\sum_{\beta=a,b}\left[\frac{(p^\beta)^2}{2m}+V^\beta\left(x^\beta-\bar{x}^\beta(t)\right)\right]+V_{\mathrm{int}}^{\mathrm{ab}}(x^a-x^b). \tag{8}$$

Here, $V^{a,b}(x^{a,b}-\bar{x}^{a,b}(t))$ describe the displaced trap potentials and V_{int}^{ab} is the interatomic interaction potential. Ideally, we want to implement the transformation from before to after the collision,

$$\psi_0^a(x^a-\bar{x}^a)\psi_0^b(x^b-\bar{x}^b)\rightarrow \mathrm{e}^{\mathrm{i}\phi}\psi_0^a(x^a-\bar{x}^a)\psi_0^b(x^b-\bar{x}^b), \tag{9}$$

where each atom remains in the ground state of its trapping potential and preserves its internal state. The phase $\phi=\phi^a+\phi^b+\phi^{\mathrm{ab}}$ will contain a contribution ϕ^{ab} from

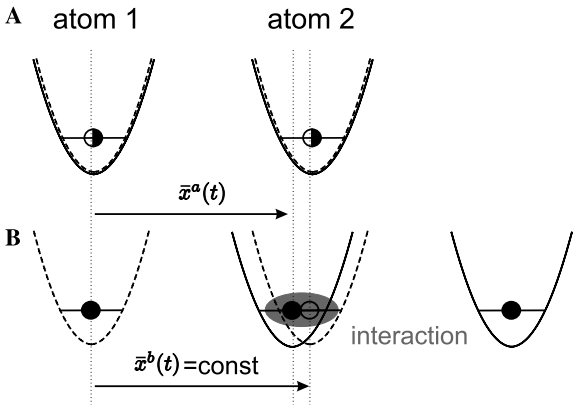

Fig. 10. We collide one atom in internal state $|a\rangle$ (filled circle, potential indicated by solid curve) with a second atom in state $|b\rangle$ (open circle, potential indicated by dashed curve)). In the collision the wave function accumulates a phase according to Eq. (9). (A) Configurations at times $t=\pm\tau$ and (B) at time t.

the interaction (collision) and (trivial) single particle kinematic phases ϕ^a and ϕ^b. The transformation (9) can be realized in the *adiabatic limit*, whereby we move the potentials slowly on the scale given by the trap frequency, so that the atoms remain in their ground state. In this case the collisional phase shift is given by $\phi^{ab} = \int_{-\infty}^{\infty} \mathrm{d}t\, \Delta E(t)$, where $\Delta E(t)$ is the energy shift induced by the atom–atom interactions, which in the case of purely s-wave scattering is given by

$$\Delta E(t) = \frac{4\pi a_s}{m} \int \mathrm{d}x\, |\psi_0^a(x - \bar{x}^a(t))|^2 |\psi_0^b(x - \bar{x}^b(t))|^2. \tag{10}$$

In addition, we assume that $|\Delta E(t)| \ll \omega_T$ so that no sloshing motion is excited.

This process of *colliding atoms by hand* can be used to create entangled states between the two atoms. By moving a state selective optical lattice potential the wave function of each atomic qubit splits up in space according to the internal superposition of states $|a\rangle$ and $|b\rangle$ as shown in cf. Fig. 10B. Only the wave function of the left atom in state $|a\rangle$ reaches the position of the second atom in state $|b\rangle$ and they will interact with each other. However, any other combination of internal states will not interact and therefore such a collision in a state selective optical lattice is conditional on the internal state.

A maximally entangled Bell state can be created by carrying out a state selective collision with a phase $\phi^{ab} = \pi$ and an initial superposition $|+\rangle \propto |a\rangle + |b\rangle$ of each atom. After the collision this state is transformed into $|a\rangle|+\rangle + |b\rangle|-\rangle$ with $|-\rangle \propto |a\rangle - |b\rangle$, i.e., $|+\rangle$ of the second atom is flipped to the orthogonal state $|-\rangle$ conditional on the state of the first atom thus creating a Bell state. Identifying $|a\rangle \equiv |0\rangle$ and $|b\rangle \equiv |1\rangle$ we obtain for the logical states the mapping $|i,j\rangle \to (-1)^{(1-i)j}|i,j\rangle$, with $i,j \in \{0,1\}$ (up to trivial phases) which realizes a two-qubit phase gate. This gate in combination with single-qubit rotations is universal, i.e., they allow to implement any unitary dynamics on a quantum register [60].

5.2. Universal quantum simulators

Building a general purpose quantum computer, which is able to run for example Shor's algorithm, requires quantum resources which will only be available in the long-term future. Thus, it is important to identify *nontrivial* applications for quantum computers with limited resources, which are available in the lab at present. Such an example is provided by *Feynman's universal quantum simulator* (UQS) [68]. A UQS is a controlled device that, operating itself on the quantum level, efficiently reproduces the dynamics of any other many-particle system that evolves according to short range interactions. Consequently, a UQS could be used to efficiently simulate the dynamics of a generic many-body system, and in this way function as a fundamental tool for research in many body physics, e.g., to simulate spin systems.

According to Jane et al. [69] the very nature of the Hamiltonian available in quantum optical systems makes them best suited for simulating the evolution of systems whose building blocks are also two-level atoms, and having a Hamiltonian $H_N = \sum_a H^{(a)} + \sum_{a \neq b} H^{(ab)}$ that decomposes into one-qubit terms $H^{(a)}$ and two-qubit terms $H^{(ab)}$. A starting observation concerning the simulation

of quantum dynamics is that if a Hamiltonian $K = \sum_{j=1}^{s} K_j$ decomposes into terms K_j acting in a small constant subspace, then by the Trotter formula $e^{-iK\tau} = \lim_{m\to\infty}(e^{-iK_1\tau/m}e^{-iK_2\tau/m}\cdots e^{-iK_s\tau/m})^m$ we can approximate an evolution according to K by a series of short evolutions according to the pieces K_j. Therefore, we can simulate the evolution of an N-qubit system according to the Hamiltonian H_N by composing short one-qubit and two-qubit evolutions generated, respectively, by $H^{(a)}$ and $H^{(ab)}$. In quantum optics an evolution according to one-qubit Hamiltonians $H^{(a)}$ can be obtained directly by properly shining a laser beam on the atoms or ions that host the qubits. Instead, two-qubit Hamiltonians are achieved by processing some given interaction $H_0^{(ab)}$ (see the example below) that is externally enforced in the following way. Let us consider two of the N qubits, that we denote by a and b. By alternating evolutions according to some available, switchable two qubit interaction $H_0^{(ab)}$ for some time with local unitary transformations, one can achieve an evolution

$$U\left(t = \sum_{j=1}^{n} t_j\right) = \prod_{j=1}^{n} V_j \exp(-iH_0^{(ab)} t_j) V_j^\dagger = \prod_{j=1}^{n} \exp(-iV_j H_0^{(ab)} V_j^\dagger t_j),$$

where $t = \sum_{j=1}^{n} t_j$, $V_j = u_j^{(a)} \otimes v_j^{(b)}$ with u_j and v_j being one-qubit unitaries. For a small time interval $U(t) \simeq 1 - it\sum_{j=1}^{n} p_j V_j H_0^{(ab)} V_j^\dagger + O(t^2)$ with $p_j = t_j/t$, so that by concatenating several short gates $U(t)$, $U(t) = \exp(-iH_{\text{eff}}^{(ab)} t) + O(t^2)$, we can simulate the Hamiltonian

$$H_{\text{eff}}^{(ab)} = \sum_{j=1}^{n} p_j V_j H_0^{(ab)} V_j^\dagger + O(t)$$

for larger times. Note that the systems can be classified according to the availability of homogeneous manipulation, $u_j = v_j$, or the availability of local individual addressing of the qubits, $u_j \neq v_j$.

Cold atoms in optical lattices provide an example where single atoms can be loaded with high fidelity into each lattice site, and where cold controlled collisions provide a way of entangling these atoms in a highly parallel way. This assumes that atoms have two internal (ground) states $|0\rangle \equiv |\downarrow\rangle$ and $|1\rangle \equiv |\uparrow\rangle$ representing a qubit, and that we have two *spin-dependent* lattices, one trapping the $|0\rangle$ state, and the second supporting the $|1\rangle$. An interaction between adjacent qubits is achieved by displacing one of the lattices with respect to the other as discussed in the previous subsection. In this way the $|0\rangle$ component of the atom a approaches in space the $|1\rangle$ component of atom $a+1$, and these collide in a controlled way. Then the two components of each atom are brought back together. This provides an example of implementing an Ising $\sum_{a\neq b} H_0^{(ab)} = \sum_a \sigma_z^{(a)} \otimes \sigma_z^{(a+1)}$ interaction between the qubits, where the $\sigma^{(a)'}$s denote Pauli matrices. By a sufficiently large, relative displacement of the two lattices, also interactions between more distant qubits could be achieved. A local unitary transformation can be enforced by shining a laser on the atoms, inducing an arbitrary rotation between $|0\rangle$ and $|1\rangle$. On the time scale of the collisions requiring a displacement of the lattice (the entanglement operation) these local operations can

be assumed instantaneous. In the optical lattice example it is difficult to achieve an individual addressing of the qubits. Such an addressing would be available in an ion trap array as discussed in [70]. These operations provide us with the building blocks to obtain an effective Hamiltonian evolution by time averaging as outlined above.

As an example let us consider the ferromagnetic [antiferromagnetic] Heisenberg Hamiltonian $H = J\sum_{j=x,y,z}\sigma_j \otimes \sigma_j$ where $J > 0$ [$J < 0$]. An evolution can be simulated by short gates with $H_0^{(ab)} = \gamma\sigma_z \otimes \sigma_z$ alternated with local unitary operations

$$p_1 = \frac{1}{3}, \quad V_1 = \hat{1} \otimes \hat{1},$$

$$p_2 = \frac{1}{3}, \quad V_2 = \frac{\hat{1} - i\sigma_x}{\sqrt{2}} \otimes \frac{\hat{1} - i\sigma_x}{\sqrt{2}},$$

$$p_3 = \frac{1}{3}, \quad V_3 = \frac{\hat{1} - i\sigma_y}{\sqrt{2}} \otimes \frac{\hat{1} - i\sigma_y}{\sqrt{2}}$$

without local addressing, as provided by the standard optical lattice setup. The ability to perform independent operations on each of the qubits would translate into the possibility to simulate any bipartite Hamiltonians.

An interesting aspect is the possibility to simulate effectively different lattice configurations: for example, in a 2D pattern a system with nearest neighbor interactions in a triangular configuration can be obtained from a rectangular array configuration. This is achieved by making the subsystems in the rectangular array interact not only with their nearest neighbor but also with two of their next-to-nearest neighbors in the same diagonal (see Fig. 11).

One of the first and most interesting applications of quantum simulations is the study of quantum phase transitions [71]. In this case one would obtain the ground state of a system, adiabatically connecting ground states of systems in different regimes of coupling parameters, allowing to determine its properties.

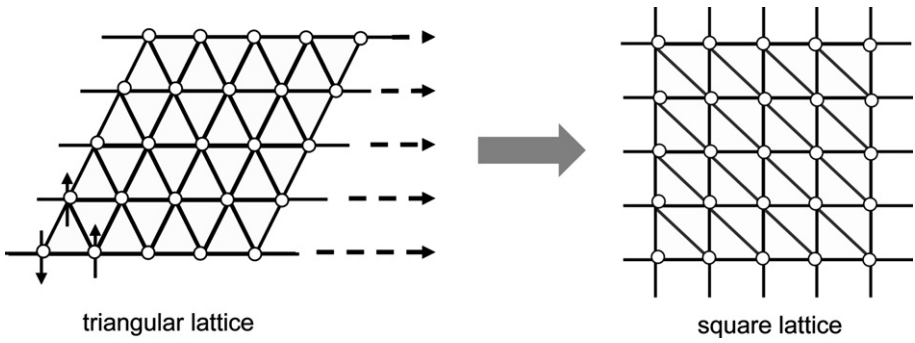

Fig. 11. Illustration how triangular configurations of atoms with nearest neighbor interactions may be simulated in a rectangular lattice.

6. Impurities and atomic quantum dots

A focused laser beam superimposed to a trap holding a quantum degenerate bose or fermi gas can form a tight local trapping potential, which can play the role of an *impurity site*, or an *atomic quantum dot*, coupled to a cold atom reservoir [72,73]. This opens the possibility of studying impurity physics or the analogue of quantum dot physics with quantum degenerate gases with controllable external parameters, and has several interesting applications, e.g., extraction of single atoms from an atomic BEC. Impurity potentials can be created as a local deformation of the original trap holding the atomic gas with tunnel coupling between reservoir and the dimple, or with a spin-dependent potential. In the latter case, atoms in the internal state $|a\rangle$ see only the large trap representing the reservoir, while atoms in state $|b\rangle$ are held by the local tight trap. Coupling of atoms occupying the atomic quantum dot to the reservoir of b-atoms is achieved via a Raman transition (Fig. 12). Depending on the choice of the trapping potential for the reservoir atoms, we can realize configurations, where the dot is coupled to a reservoir of a 1D (Luttinger), 2D or 3D quantum gas. Atoms occupying the dot and the reservoir will interact via collisional interactions. In particular, in the limit of a tight trap representing the dot and strong repulsion between the atoms we can have a situation of a *collisional blockade regime* [73], where only a single atom can occupy the dot, in analogy to the Coulomb blockade in electronic quantum dots. In the following we will consider two specific examples to illustrate these configurations. Again our emphasis will be on the derivation of the corresponding Hamiltonians, while we refer to the original papers for a discussion of the system dynamics.

6.1. Atomic quantum dot coupled to superfluid reservoir: quantum engineering of a spin-boson model

As our first example, we consider the configuration outlined in Fig. 12 where a superfluid reservoir of Bose atoms in internal state $|a\rangle$ is coupled via Raman

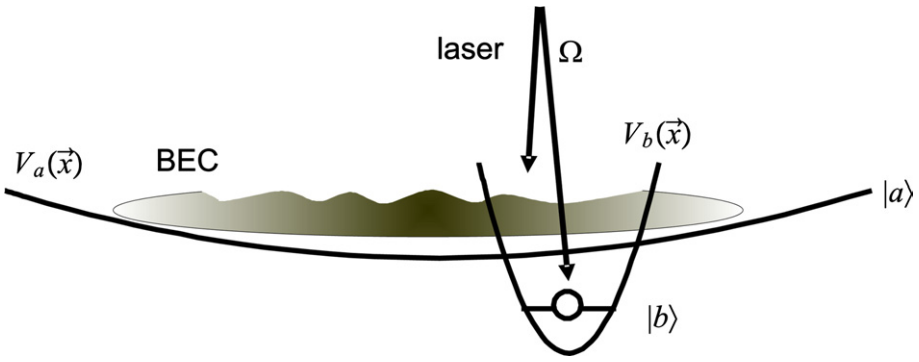

Fig. 12. Schematic setup of an atomic quantum dot coupled to a superfluid atomic reservoir. The Bose-liquid of atoms in state $|a\rangle$ is confined in a shallow trap $V_a(\mathbf{x})$. The atom in state $|b\rangle$ is localized in a tightly confining potential $V_b(\mathbf{x})$. Atoms in state $|a\rangle$ and $|b\rangle$ are coupled via a Raman transition with effective Rabi frequency Ω. A large onsite interaction $U_{bb} > 0$ allows only a single atom in the dot.

transitions to the lowest vibrational state of an atomic quantum dot with atoms in state $|b\rangle$ [73]. The resulting dynamics will be described by a *spin-Boson model* [74], where the occupation of the dot (represented by a pseudo-spin) is coupled to the density and phase fluctuations of the superfluid. The distinguishing features of the model are: (i) the control of the spin-phonon bath coupling by the collisional parameters, and (ii) the realization of an ohmic or superohmic reservoir. As a result, the rich dynamics for the spin-Boson model, for example dissipative phase transitions, should be observable in the quantum dot dynamics.

The collisional interaction of atoms in the two internal levels are described by a set of parameters $g_{\alpha\beta} = 4\pi\, a_{\alpha\beta}/m$ with scattering lengths $a_{\alpha\beta}$ ($\alpha,\beta = a,b$). Following steps analogous to the derivation of the BHM Hamiltonian in Section 3 we arrive at the Hamiltonian for the dot H_b and its coupling to the reservoir H_{ab},

$$H_b + H_{ab} = \left(-\delta + g_{ab}\int \mathrm{d}\mathbf{x}|\psi_b(\mathbf{x})|^2\hat{\rho}_a(\mathbf{x})\right)\hat{b}^\dagger\hat{b} + \frac{U_{bb}}{2}\hat{b}^\dagger\hat{b}^\dagger\hat{b}\hat{b} + \int \mathrm{d}\mathbf{x}\,\Omega(\hat{\Psi}_a(\mathbf{x})\psi_b(\mathbf{x})\hat{b}^\dagger + \text{h.c.}). \tag{11}$$

Here, $\hat{b}$ is the bosonic destruction operator for b-atom in the lowest vibrational state of the dot with wave function $\psi_b(\mathbf{x})$, while $\hat{\Psi}_a(\mathbf{x})$ is the annihilation operator for a reservoir atom a at point $\mathbf{x}$. The first term in (11) contains the Raman detuning δ and the collisional shift of the lowest vibrational state of the dot due to interaction with the reservoir with atomic density $\hat{\rho}_a(\mathbf{x}) = \hat{\Psi}_a^\dagger(\mathbf{x})\hat{\Psi}_a(\mathbf{x})$. The second term is the onsite repulsion U_{bb} of the atoms occupying the quantum dot, and the third term is the laser induced coupling transferring atoms from the dot to the reservoir with effective two-photon Rabi frequency Ω.

At sufficiently low temperatures the reservoir atoms in $|a\rangle$ form a superfluid Bose liquid with an equilibrium liquid density ρ_a. The only available excitations at low energies are then phonons with linear dispersion $\omega = v_s|\mathbf{q}|$ and sound velocity v_s. We write the atomic density operator in terms of the density fluctuation operator $\hat{\Pi}$, $\hat{\rho}_a(\mathbf{x}) = \rho_a + \hat{\Pi}(\mathbf{x})$, which is canonically conjugate to the superfluid phase $\hat{\phi}(\mathbf{x})$ with $\hat{\Psi}_a \sim \hat{\rho}_a^{1/2}\mathrm{e}^{-\mathrm{i}\hat{\phi}}$. In the long wavelength approximation the dynamics of the superfluid is described by a (quantum) hydrodynamic Hamiltonian, $\hat{H}_a = v_s\sum_{\mathbf{q}}|\mathbf{q}|\hat{b}_{\mathbf{q}}^\dagger\hat{b}_{\mathbf{q}}$, which has the form of a collection of harmonic sound modes with annihilation operators of phonons $\hat{b}_{\mathbf{q}}$. Since the excitations of a weakly interacting Bose-liquid are phonon-like only for wavelengths larger than the healing length $\xi \geqslant l_b$, the summation over the phonon modes is cutoff at a frequency $\omega_c = v_s/\xi \approx g_{aa}\rho_a$.

In the collisional blockade limit of large onsite interaction U_{bb} only states with occupation $n_b = 0$ and 1 in the dot participate in the dynamics, while higher occupations are suppressed by the large collisional shift. This situation and its description is analogous to the Mott insulator limit in optical lattices. Thus, the quantum state of a dot is described by a pseudo-spin-1/2, with the spin-up or spin-down state corresponding to occupation by a single or no atom in the dot. Using standard Pauli matrix notation, the dot occupation operator $\hat{b}^\dagger\hat{b}$ is then replaced by $(1+\sigma_z)/2$ while $\hat{b}^\dagger \to \sigma_+$. Furthermore, for the long wavelength wavevectors $|\mathbf{q}|l_b \ll 1$ with l_b the

dimension of the dot, the phonon field operators may be replaced by their values at $\mathbf{x} = \mathbf{0}$. This gives the Hamiltonian

$$\hat{H}_b + \hat{H}_{ab} = \left(-\frac{\delta}{2} + \frac{g_{ab}}{2}\hat{\Pi}(\mathbf{0})\right)\sigma_z + \frac{\Delta}{2}(\sigma_+ e^{-i\hat{\phi}(\mathbf{0})} + \text{h.c.}). \tag{12}$$

Here, $\Delta \sim \Omega n_a^{1/2}$ is an effective Rabi frequency with n_a the number of bosons inside the quantum dot wave function ψ_b. An important feature of this Hamiltonian is that phonons couple to the dot dynamics via: (i) the collisional interactions coupling to the density fluctuations $\hat{\Pi}(\mathbf{0})$, and (ii) to the superfluid phase $\hat{\phi}(\mathbf{0})$ via the laser couplings. A unitary transformation $\hat{H} = \hat{S}^{-1}(\hat{H}_a + \hat{H}_b + \hat{H}_{ab})\hat{S}$ with $\hat{S} = \exp(-\sigma_z i\hat{\phi}(\mathbf{0})/2)$ transforms the phase fluctuations in the Rabi term to a frequency fluctuation which adds this contribution to the first term in (12). Thus, the dynamics of the quantum dot coupled to the superfluid reservoir gives rise to a *spin-Boson Hamiltonian* [74]

$$\hat{H} = \sum_{\mathbf{q}} \omega_{\mathbf{q}} b_{\mathbf{q}}^\dagger b_{\mathbf{q}} + \left(-\delta + \sum_{\mathbf{q}} \lambda_{\mathbf{q}}(\hat{b}_{\mathbf{q}} + \hat{b}_{\mathbf{q}}^\dagger)\right)\frac{\sigma_z}{2} - \frac{\Delta}{2}\sigma_x \tag{13}$$

with amplitudes of the total phonon coupling $\lambda_{\mathbf{q}} = |m\mathbf{q}v_s^3/2V\rho_a|^{1/2}(g_{ab}\rho_a/mv_s^2 - 1)$, as a sum of the collisional interaction g_{ab} and the transformed phase fluctuations. We note the following two features of the model.

6.1.1. Control of spin-bath coupling by quantum interference

For a repulsive inter-species interaction, $g_{ab} > 0$, both contributions in λ_q interfere destructively: the effect of the phonon excitation in a laser-driven transition $a \leftrightarrow b$ can be precisely cancelled by the change in the direct "elastic" interaction between the liquid and the b atoms, as described by the first term in Eq. (12). In a weakly interacting gas $mv_s^2 = \rho_a g_{aa}$ and thus the coupling constants $\lambda_{\mathbf{q}}$ vanish at $g_{ab} = g_{aa}$. At this special point, we have thus decoupled the dissipative phonon reservoir from the spin, i.e., we have stable superposition of occupation and non-occupation of the dot, exhibiting undamped Rabi oscillations of the quantum dot's occupancy.

6.1.2. Ohmic and superohmic bath couplings

The system is characterized by the effective density of states $J(\omega) = \sum_{\mathbf{q}} \lambda_{\mathbf{q}}^2 \delta(\omega - \omega_{\mathbf{q}}) = 2\alpha\omega^s$, where $\alpha \sim (g_{ab}\rho_a/mv_s^s - 1)^2$ is the dissipation strength due to the spin-phonon coupling and $D = s$ the dimension of the superfluid reservoir. In the standard terminology [74], $s = 1$ and $s > 1$ correspond to the ohmic and superohmic cases, respectively.

For a discussion of the dynamics and the validity of the model, and specific atomic realizations we refer to [73,74].

6.2. A "single atom transistor" with a 1D optical lattice

As a second example, we consider a spin-1/2 atomic impurity which is used to switch the transport of either a 1D Bose-Einstein Condensate (BEC) or a 1D degenerate Fermi gas initially situated to one side of the impurity [75]. In one spin state the impurity is transparent to the probe atoms, while in the other it acts as single atom

mirror prohibiting transport. Observation of the atomic current passing the impurity can then be used as a quantum non-demolition measurement of its internal state, which can be seen to encode a qubit, $|\psi_q\rangle = \alpha\,|\uparrow\rangle + \beta|\downarrow\rangle$. If a macroscopic number of atoms pass the impurity, then the system will be in a macroscopic superposition, $|\Psi(t)\rangle = \alpha\,|\uparrow\rangle|\phi_\uparrow(t)\rangle + \beta|\downarrow\rangle|\phi_\downarrow(t)\rangle$, which can form the basis for a single shot readout of the qubit spin. Here, $|\phi_\sigma(t)\rangle$ denotes the state of the probe atoms after evolution to time t, given that the qubit is in state σ (Fig. 13A). In view of the analogy between state amplification via this type of blocking mechanism and readout with single electron transistors (SET) used in solid state systems, we refer to this setup as a single atom transistor (SAT).

We consider the implementation of a SAT using cold atoms in 1D optical lattices: probe atoms in state $|b\rangle$ are loaded in the lattice to the left of a site containing the impurity atom $|q\rangle$, which is trapped by a separate (e.g., spin-dependent) potential (Fig. 13B). The passage of $|b\rangle$ atoms past the impurity q is then governed by the spin-dependent effective collisional interaction $\hat{H}_{\rm int} = \sum_\sigma U_{{\rm eff},\sigma}\hat{b}_0^\dagger\hat{b}_0\hat{q}_\sigma^\dagger\hat{q}_\sigma$. By making use of a quantum interference mechanism, we engineer complete blocking (effectively $U_{\rm eff}\to\infty$) for one spin state and complete transmission ($U_{\rm eff}\to 0$) for the other.

The quantum interference mechanism needed to engineer $U_{\rm eff}$ can be produced using an optical or magnetic Feshbach resonance [42,45,46], and we use the present example to illustrate Hamiltonians for impurity interactions involving Feshbach resonances and molecular interactions. For the optical case a Raman laser drives a transition on the impurity site, 0, from the atomic state $\hat{b}_0^\dagger\hat{q}_\sigma^\dagger|{\rm vac}\rangle$ via an off-resonant excited molecular state to a bound molecular state back in the lowest electronic manifold $\hat{m}_\sigma^\dagger|{\rm vac}\rangle$ (Fig. 14A). We denote the effective two-photon Rabi frequency and detuning by Ω_σ and Δ_σ, respectively. The Hamiltonian for our system is then given by $\hat{H} = \hat{H}_b + \hat{H}_0$, with

$$\hat{H}_b = -J\sum_{\langle ij\rangle}\hat{b}_i^\dagger\hat{b}_j + \frac{1}{2}U_{bb}\sum_j\hat{b}_j^\dagger\hat{b}_j(\hat{b}_j^\dagger\hat{b}_j - 1), \tag{14}$$

$$\hat{H}_0 = \sum_\sigma[\Omega_\sigma(\hat{m}_\sigma^\dagger\hat{q}_\sigma\hat{b}_0 + {\rm h.c.}) - \Delta_\sigma\hat{m}_\sigma^\dagger\hat{m}_\sigma] + \sum_\sigma[U_{qb,\sigma}\hat{b}_0^\dagger\hat{q}_\sigma^\dagger\hat{q}_\sigma\hat{b}_0 + U_{bm,\sigma}\hat{b}_0^\dagger\hat{m}_\sigma^\dagger\hat{m}_\sigma\hat{b}_0]. \tag{15}$$

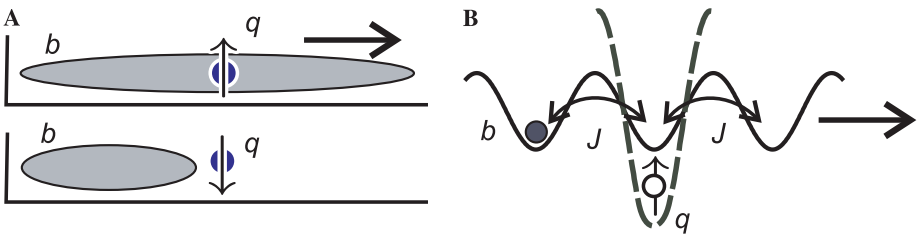

Fig. 13. (A) A spin 1/2 impurity used as a switch: in one spin state it is transparent to the probe atoms, but in the other it acts as a single atom mirror. (B) Implementation of the SAT as a separately trapped impurity q with probe atoms b in an optical lattice.

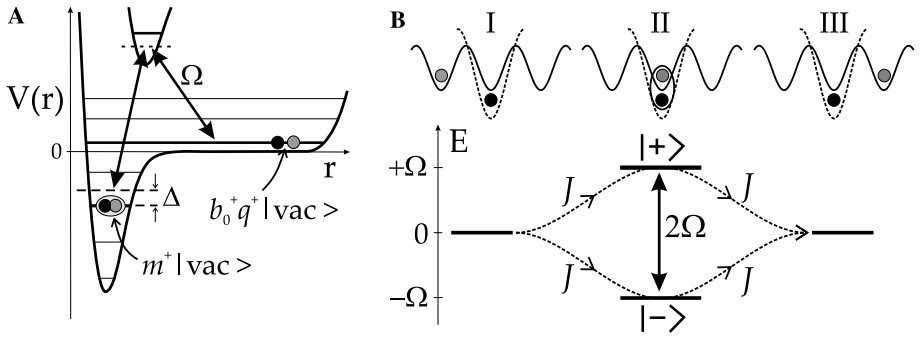

Fig. 14. (A) The optical Feshbach setup couples the atomic state $\hat{b}_0^\dagger \hat{q}_\sigma^\dagger|\text{vac}\rangle$ (in a particular motional state quantized by the trap) to a molecular bound state of the Born–Oppenheimer potential, $m_\sigma^\dagger|\text{vac}\rangle$, with effective Rabi frequency Ω_σ and detuning Δ_σ. (B) A single atom passes the impurity (I $\to$ III) via the two dressed states (II), $|+\rangle = \hat{b}_0^\dagger \hat{q}_\sigma^\dagger|\text{vac}\rangle + m_\sigma^\dagger|\text{vac}\rangle$ and $|-\rangle = \hat{b}_0^\dagger \hat{q}_\sigma^\dagger|\text{vac}\rangle - m_\sigma^\dagger|\text{vac}\rangle$. Quantum interference between the paths gives rise to an effective tunnelling rate $J_{\text{eff},\sigma}$.

Here, $\hat{H}_\text{b}$ is a familiar Hubbard Hamiltonian for atoms in state $|b\rangle$; $\hat{H}_0$ describes the additional dynamics due to the impurity on site 0, where atoms in state $|b\rangle$ and $|q\rangle$ are converted to a molecular state with effective Rabi frequency Ω_σ and detuning Δ_σ, and the last two terms describe background interactions, $U_{\alpha\beta,\sigma}$ for two particles $\alpha,\beta \in \{q_\sigma, b, m\}$, which are typically weak. This model is valid for $U_{\alpha\beta}, J, \Omega, \Delta \ll \omega_T$ (where ω_T is the energy separation between Bloch bands). Because the dynamics for the two spin channels q_σ can be treated independently, in the following we will consider a single spin channel, and drop the subscript σ.

To understand the qualitative physics behind the above Hamiltonian, let us consider the molecular couplings and associated effective interactions between the $|q\rangle$ and $|b\rangle$ atoms for: (i) off-resonant ($\Omega \ll |\Delta|$) and (ii) resonant ($\Delta = 0$) laser driving. In the first case the effective interaction between $|b\rangle$ and $|q\rangle$ atoms is $U_{\text{eff}} = U_{qb} + \Omega^2/\Delta$, where the second term is an AC Stark shift which plays the role of the resonant enhancement of the collisional interactions between $|b\rangle$ and $|q\rangle$ atoms due to the optical Feshbach resonance. For resonant driving ($\Delta = 0$) the physical mechanism changes. On the impurity site, laser driving mixes the states $\hat{b}_0^\dagger \hat{q}^\dagger|\text{vac}\rangle$ and $m^\dagger|\text{vac}\rangle$, forming two dressed states with energies $\varepsilon_\pm = (U_{qb})/2 \pm (U_{qb}^2/4 + \Omega^2)^{1/2}$ (Fig. 14B, II). Thus we have two interfering quantum paths via the two dressed states for the transport of $|b\rangle$ atoms past the impurity. In the simple case of weak tunneling $\Omega \gg J$ and $U_{qb} = 0$ second-order perturbation theory gives for the effective tunnelling $J_\text{eff} = -(J^2/\varepsilon + \Omega) - (J^2/\varepsilon - \Omega) \to 0$ ($|\varepsilon| \ll \Omega$) which shows destructive quantum interference, analogous to the interference effect underlying electromagnetically induced transparency (EIT) [76], and is equivalent to having an effective interaction $U_\text{eff} \to \infty$.

In [75] the exact dynamics for scattering of a single $|b\rangle$ atom from the impurity is solved exactly, confirming the above qualitative picture of EIT-type quantum interference. Furthermore, in this reference a detailed study of the time-dependent many

body dynamics based on the 1D Hamiltonian (15) is presented for interacting many-particle systems including a 1D Tonks gas.

7. Conclusions

The cold atom Hubbard toolbox presented in this paper opens a range of novel and exciting prospects for controlling and manipulating strongly correlated atomic systems. The resulting standard and exotic many body Hamiltonians can be used to simulate otherwise untractable systems in condensed matter physics. The *quantum simulation* of such systems becomes feasible with cold atoms and provides a valuable tool which can be used in addition to standard analytical and numerical methods for analyzing many body systems. In addition, we have shown that they also pose new challenges like, e.g., understanding and utilizing the unitary dynamics that can be realized in optical lattices.

References

[1] For a review see, Nature 416 (2002) 205–246.
[2] F. Dalfovo, S. Giorgini, L. Pitaevskii, S. Stringari, Rev. Mod. Phys. 71 (1999) 463.
[3] A. Leggett, Rev. Mod. Phys. 73 (2001) 307.
[4] L. Pitaevskii, S. Stringari, Bose-Einstein Condensation, Oxford University Press, Oxford, 2003.
[5] C. Pethick, H. Smith, Bose-Einstein Condensation in Dilute Gases, Cambridge University Press, Cambridge, 2001.
[6] D. Jaksch, C. Bruder, J. Cirac, C. Gardiner, P. Zoller, Phys. Rev. Lett. 81 (15) (1998) 3108.
[7] M. Greiner, O. Mandel, T. Esslinger, T. Hänsch, I. Bloch, Nature 415 (2002) 39.
[8] J.I. Cirac, P. Zoller, Phys. Today (2004) 38–44.
[9] H. Metcalf, P. van der Straten, Laser Cooling and Trapping, Springer, New York, 1999.
[10] P. Jessen, I. Deutsch, Adv. At. Mol. Opt. Phys. 37 (1996) 95.
[11] W. Kohn, Phys. Rev. 115 (1959) 809.
[12] D. Jaksch, H. Briegel, J. Cirac, C. Gardiner, P. Zoller, Phys. Rev. Lett. 82 (1999) 1975.
[13] G. Brennen, C. Caves, P. Jessen, I. Deutsch, Phys. Rev. Lett. 82 (1999) 1060.
[14] W. Liu, F. Wilczek, P. Zoller, Phys. Rev. A 70 (2004) 033603.
[15] M. Fisher, P. Weichman, G. Grinstein, D. Fisher, Phys. Rev. B 40 (1989) 546.
[16] W. Hofstetter, J.I. Cirac, P. Zoller, E. Demler, M. Lukin, Phys. Rev. Lett. 89 (2002) 220407.
[17] L. Santos, M.A. Baranov, J. Cirac, H.-U. Everts, H. Fehrmann, M. Lewenstein, Phys. Rev. Lett. 93 (2004) 030601.
[18] B. Damski, J. Zakrzewski, L. Santos, P. Zoller, M. Lewenstein, Phys. Rev. Lett. 91 (2003) 080403.
[19] B. Paredes, A. Widera, V. Murg, O. Mandel, S. Fölling, I. Cirac, G.V. Shlyapnikov, T.W. Hänsch, I. Bloch, Nature 429 (2004) 277–281.
[20] T. Stöferle, H. Moritz, C. Schori, M. Köhl, T. Esslinger, Phys. Rev. Lett. 92 (2004) 130403.
[21] A. Kuklov, N. Prokof'ev, B. Svistunov, Phys. Rev. Lett. 92 (2004) 050402.
[22] A. Sorensen, K. Molmer, Phys. Rev. Lett. 83 (1999) 2274–2277.
[23] L.-M. Duan, E. Demler, M. Lukin, Phys. Rev. Lett. 91 (2003) 090402.
[24] J.K. Pachos, M.B. Plenio, Phys. Rev. Lett. 93 (2004) 056402.
[25] B. Paredes, J.I. Cirac, Phys. Rev. Lett. 90 (2003) 150402.
[26] R. Roth, K. Burnett, Phys. Rev. A 69 (2004) 021601.
[27] M. Lewenstein, L. Santos, M. Baranov, H. Fehrmann, Phys. Rev. Lett. 92 (2004) 050401.
[28] H. Büchler, G. Blatter, Phys. Rev. A 69 (2004) 063603.

[29] D. Jaksch, P. Zoller, New J. Phys. 5 (2003) 56.
[30] D. Hofstadter, Phys. Rev. B 14 (1976) 2239.
[31] A.S. Sorensen, E. Demler, M.D. Lukin. Available from: <cond-mat/0405079>.
[32] J.-P. Martikainen, H. Stoof, Phys. Rev. A 69 (2004) 053617.
[33] A. Smerzi, A. Trombettoni, P. Kevrekidis, A.R. Bishop, Phys. Rev. Lett. 89 (2002) 170402.
[34] C. Menotti, M. Krämer, L. Pitaevskii, S. Stringari, Phys. Rev. A 67 (2003) 053609.
[35] B. Anderson, M. Kasevich, Science 282 (1998) 1686.
[36] O. Morsch, J. Müller, M. Cristiani, D. Ciampini, E. Arimondo, Phys. Rev. Lett. 87 (2001) 140402.
[37] W. Hensinger, H. Haffner, A. Browaeys, N.R. Heckenberg, K. Helmerson, C. McKenzie, G.J. Milburn, W.D. Phillips, S.L. Rolston, H. Rubinsztein-Dunlop, B. Upcroft, Nature 412 (2001) 52.
[38] D.A. Steck, W.H. Oskay, M.G. Raizen, Science 293 (2001) 274–278.
[39] S. Peil, J. Porto, B.L. Tolra, J. Obrecht, B. King, M. Subbotin, S. Rolston, W. Phillips, Phys. Rev. A 67 (2003) 051603.
[40] P. Rabl, A.J. Daley, P.O. Fedichev, J.I. Cirac, P. Zoller, Phys. Rev. Lett. 91 (2003) 110403.
[41] A.J. Daley, P.O. Fedichev, P. Zoller, Phys. Rev. A 69 (2004) 022306.
[42] E. Bolda, E. Tiesinga, P. Julienne, Phys. Rev. A 66 (2002) 013403.
[43] E. Bolda, E. Tiesinga, P. Julienne, Phys. Rev. A 68 (2003) 032702.
[44] J. Weiner, V. Bagnato, S. Zilio, P. Julienne, Rev. Mod. Phys. 71 (1999) 1.
[45] M. Theis, G. Thalhammer, K. Winkler, M. Hellwig, G. Ruff, R. Grimm, J.H. Denschlag, Phys. Rev. Lett. 93 (2004) 123001.
[46] T. Calarco, U. Dorner, P. Julienne, C. Williams, P. Zoller, Phys. Rev. A 70 (2004) 012306.
[47] D. Jaksch, V. Venturi, J.I. Cirac, C.J. Williams, P. Zoller, Phys. Rev. Lett. 89 (2002) 040402.
[48] D. Petrov, Phys. Rev. Lett. 93 (2004) 143201.
[49] P. Fedichev, M. Reynolds, G. Shlyapnikov, Phys. Rev. Lett. 77 (1996) 2921.
[50] B.L. Tolra, K.M. O'Hara, J. Huckans, W. Phillips, S. Rolston, J.V. Porto, Phys. Rev. Lett. 92 (2004) 190401.
[51] S. Clark, D. Jaksch, Phys. Rev. A 70 (2004) 043612.
[52] K. Braun-Munzinger, J.A. Dunningham, K. Burnett, Phys. Rev. A 69 (2004) 053613.
[53] I. Carusotto, Y. Castin, J. Dalibard, Phys. Rev. A 63 (2001) 023606.
[54] P. Drummond, P. Deuar, K. Kheruntsyan, Phys. Rev. Lett. 92 (2004) 040405.
[55] G. Vidal, Phys. Rev. Lett. 91 (2003) 147902.
[56] A. Daley, C. Kollath, U. Schollwöck, G. Vidal, J. Stat. Mech.: Theor. Exp. (2004) P04005.
[57] M. Cazalilla, J. Marston, Phys. Rev. Lett. 88 (2003) 256403.
[58] U. Dorner, P. Fedichev, D. Jaksch, M. Lewenstein, P. Zoller, Phys. Rev. Lett. 91 (2003) 073601.
[59] R. Raussendorf, H.J. Briegel, Phys. Rev. Lett. 86 (2001) 5188.
[60] M. Nielsen, I. Chuang, Quantum Computation and Quantum Information, Cambridge University Press, Cambridge, 2000.
[61] D. DiVincenzo, Fortschr. Phys. 48 (2000) 771.
[62] G. Brennen, I. Deutsch, P. Jessen, Phys. Rev. A 61 (2000) 62309.
[63] O. Mandel, M. Greiner, A. Widera, T. Rom, T. Hänsch, I. Bloch, Nature 425 (2003) 937.
[64] D. Jaksch, J.I. Cirac, P. Zoller, S. Rolston, R. Cote, M.D. Lukin, Phys. Rev. Lett. 85 (2000) 2208.
[65] K. Eckert, J. Mompart, X. Yi, J. Schliemann, D. Bruš, G. Birkl, M. Lewenstein, Phys. Rev. A 66 (2002) 042317.
[66] J.K. Pachos, P.L. Knight, Phys. Rev. Lett. 91 (2003) 107902.
[67] S.C. Benjamin, S. Bose, Phys. Rev. Lett. 90 (2003) 247901.
[68] S. Lloyd, Science 273 (1996) 1073.
[69] E. Jane, G. Vidal, W. Dür, P. Zoller, J. Cirac, Quantum Inform. Comput. 3 (1) (2003) 15–37.
[70] J. I. Cirac, P. Zoller, Phys. Today (2004) 38–44. Available from: <http://www.physicstoday.org/vol-57/iss-3/contents.html>.
[71] S. Sachdev, Quantum Phase Transitions, Cambridge University Press, Cambridge, 1999.
[72] R. Diener, B. Wu, M. Raizen, Q. Niu, Phys. Rev. Lett. 89 (2002) 070401.
[73] A. Recati, P. Fedichev, W. Zwerger, J. von Delft, P. Zoller. Available from: <cond-mat/0404533>.

[74] A.J. Leggett, S. Chakravarty, A.T. Dorsey, M.P.A. Fisher, A. Garg, W. Zwerger, Rev. Mod. Phys. 59 (1987) 1.
[75] A. Micheli, A. Daley, D. Jaksch, P. Zoller, Phys. Rev. Lett. 93 (2004) 140408.
[76] M. Lukin, Rev. Mod. Phys. 75 (2003) 457.